Understanding hydrogen embrittlement (HE) of line pipe steel grades tested in gaseous H2 environment

TUHIN DAS (*) (1) , NIKOLAOS VOUDOURIS (2) , SOFIA RAPTI (2) , STEVEN COOREMAN (1) , NURIA SANCHEZ (1) , ATHANASIOS TAZEDAKIS (2) , FREDERIC BOUCHAUD (3)

(1) ArcelorMittal Global Research and Development (OCAS N.V.), Pres. J.F. Kennedylaan 3, 9060 Zelzate, Belgium

(2) Corinth Pipe Works (CPW) Research & Development, VI.PE. Thisvis, 320 10 Domvrena Viotia, Greece

(3) ArcelorMittal Europe, Customer Technical Support Energy Pipes, Batiment L9, 13776 Fos-sur-Mer, France

(*) *(corresponding author)*
tuhin.das@arcelormittal.com

ABSTRACT

As the global energy landscape transitions toward hydrogen, understanding the impact of hydrogen on the fracture behavior of pipeline steels is essential for the safe deployment of hydrogen infrastructure. Hydrogen embrittlement (HE) presents a significant challenge to the integrity of line-pipe steels, particularly in applications involving the transport and storage of hydrogen gas. For this purpose, fracture toughness tests of industrial grade line-pipe steels were performed using the reversing direct current electric potential difference (DCEPD) method to enable a real time crack initiation and crack growth measurement. On one side, a pipe (γ-Pipe) was tested under two different conditions to study the effect of pressure: 100 bar pure H_2 and 80% N2/20% H_2 gas mixture (100 bar). Two other pipes (Pipe X & Pipe Y) of similar strength levels but different "thickness-to-outer diameter" ratios were tested in 100 bar H_2. The influence of H_2 partial pressure on fracture toughness appears to be present, and a negative trend between the "thickness-to-outer diameter" ratio and fracture toughness also seems possible. To advance further understanding, the fracture toughness tested samples were studied using fracture surface mapping and advanced characterization techniques. The objective is to bridge the knowledge gaps for evolving gaseous testing methodologies by focusing on the interplay between local stress-state and hydrogen concentration at the crack tip leveraging finite element analysis (FEA), while developing fundamental understanding on the HE mechanisms. A detailed fracture surface mapping of the pipes reveal that their morphology is affected by HE when tested in 100 bar H_2 compared to the ductile dimple morphology of their air tested counterparts. Several out-of-plane "secondary cracks", perpendicular to the primary crack propagation direction was observed both in the stretch zone (or boundary) and crack extension zone in the fracture surface. A good correlation was observed between the fracture toughness results and the stretch zone morphology and secondary crack formation. An advance postmortem analysis into the mechanism(s) of the secondary crack formation reveal that these cracks are associated with hydrogen enhanced dislocation activity just underneath the fracture surface, leading towards hydrogen enhanced localized plasticity (HELP) mechanism. A quantitative comparison of the total secondary crack area using a machine learning approach rooted in computer vision suggests more secondary crack formation results in lower crack growth resistance.

1. INTRODUCTION

The drive towards a global energy transition has emphasized hydrogen as a clean energy carrier. Blending hydrogen with natural gas for pipeline transportation is currently under investigation in the energy sector, as it enables the use of existing pipeline infrastructure while reducing carbon emissions in a cost-efficient manner. This approach is viewed as an effective step toward widespread hydrogen implementation alongside the construction of new pipeline infrastructure, especially in the EU and globally, as highlighted in a recent International Energy Agency (IEA) report [1] . Despite its potential, hydrogen transport presents substantial challenges regarding the material integrity of pipelines. Hydrogen embrittlement (HE) is a primary concern for line-pipe steels, as it can impair their fatigue and fracture resistance. This risk necessitates conservative operational practices and large safety margins in hydrogen storage and distribution. Consequently, understanding the fracture characteristics of pipeline steels in gaseous hydrogen environments is essential for safe and reliable infrastructure design and operation. The fracture toughness of line-pipe steels under hydrogen exposure is influenced by several factors: microstructure, yield strength, hydrogen pressure, etc. For instance, high-strength steels tend to experience a greater reduction in fracture toughness and become susceptible to HE even at lower hydrogen pressures [2] . It is also understood that higher H_2 pressures are more detrimental when pipeline steels of similar strength levels and microstructure are considered [2][3] .

While macro-scale effects of HE has been extensively studied, the atomistic interactions between hydrogen and specific microstructural features (such as dislocations, inclusions, and phase boundaries) remain poorly understood. This gap is even more pronounced in relation to critical mechanical tests used during material qualification. Established methodologies to evaluate HE based on fracture toughness testing in gaseous hydrogen environments are still evolving, with a lack of fundamental understanding of the synergistic roles of stress-state and hydrogen concentration, in particular. Bridging these knowledge gaps are essential, as microstructural engineering coupled with accurate HE evaluation is key for developing next-generation steels, as well as qualifying current pipeline steels for hydrogen applications. To advance this understanding, the present approach centers on detailed postmortem analysis of fracture toughness tested line-pipe steels in H_2. On one side, a pipe (γ-Pipe) was tested under two different conditions to study the effect of pressure: 100 bar pure H_2 and 80% N_2/20% H_2 gas mixture (100 bar). On the other side, two pipes (Pipe X & Pipe Y) of similar strength levels but different thickness/outer dia. ratios were tested at 100 bar hydrogen pressure. The fracture toughness tested samples were further studied through fracture surface mapping, advanced characterization and machine learning (ML) techniques. A good correlation was observed between the fracture toughness results and fracture surface features from the advance postmortem analysis. The local stresses and hydrogen concentrations were further investigated in relation to the fracture toughness tests by leveraging a stress coupled hydrogen diffusion finite element model.

2. FRACTURE TOUGHNESS TESTS

Rising Load Fracture Toughness Testing was performed as per ASTM E1820-22 [4] , at Corinth Pipe Works's (CPW's) hydrogen autoclave laboratory using a hydrogen gas purity of 6.0 and ambient temperature. To achieve a pure H_2 environment, a rigorous purging protocol was implemented including multiple pressurization and depressurization cycles, initially with inert gases such as nitrogen, followed by sequential high-purity hydrogen replenishments. Tests with a monotonically increasing stress intensity was used to determine the threshold fracture toughness from J-integral vs. crack extension (J-R) curves.

Standard compact tension (CT) specimens were prepared as per ASTM E1820 Annex A2 (Fig. 1 (a)), with a thickness (B) of 12.7 mm (0.5") and width-to-thickness (W/B) ratio of 4. Orientation of the CT specimens w.r.t the parent material is shown in

Fig. 1 (b). The specimens were side grooved with a reduction of 0.20B (10% per side) and groove root radius of 0.5 ± 0.2 mm, with an included angle below 90°. Side grooves were introduced after fatigue pre-cracking, with the groove root aligned along the specimen centreline ensuring symmetry. Fatigue pre-cracking was conducted in air using a crack mouth opening displacement (CMOD) extensometer such that the pre-crack depth is at least 0.1B or 1 mm (whichever was greater). The final normalized crack length (a_0/W) was maintained at 0.45-0.55 ensuring valid fracture toughness measurements. CMOD was controlled via an actuator and measured using Linear Variable Differential Transformer (LVDT) sensors. Crack growth was monitored using the reversing direct current electric potential difference (DCEPD) method.

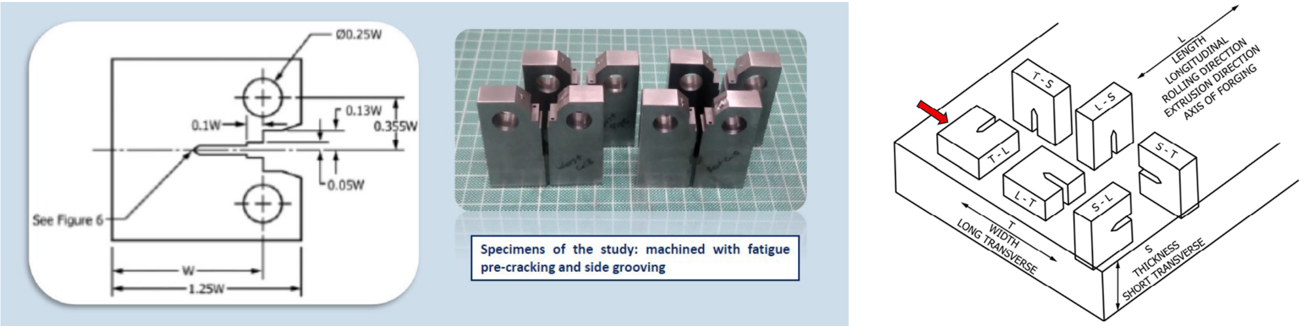

Figure 1 - CT specimen geometry, (b) CT sample orientation marked by red arrow

3. RESULTS

3.1. General characterization

All materials for this research were industrially produced by ArcelorMittal Europe as hot-rolled coils with varying thicknesses, following the thermomechanical controlled processing (TMCP) route to obtain the targeted microstructure and mechanical properties. The coils were then used to manufacture pipes at the pipe mills of CPW, of required diameter. A set of samples/coupons were extracted from the high frequency induction (HFI) welded pipes directly as "γ-Pipe", "Pipe X" and "Pipe Y". The overall microstructure of the low carbon steel samples is bainitic ferrite type, with similar phase fraction of pearlite and cementite, and comparable grain sizes. Based on the evaluation methodology described in ISO 4967 (method B, appendix C) [5], the steels have comparable cleanliness indices. The general properties for the coil and pipe samples are summarized in Table 1. The yield strengths (YS) for Pipe X and Pipe Y are similar while the YS of γ-Pipe is significantly lower compared to the others. The thickness-to-outer diameter ratio, "t/OD", for Pipe Y is twice compared to Pipe X while for γ-Pipe, it is somewhere in-between. The results from the fracture toughness tests will follow in the next section.

Table 1 - Properties of pipes and coils

Material	Thickness (t), mm	Outer diameter, inch (mm)	t/OD	P_{cm}	Yield strength, YS (MPa)	YS/TS
γ-Pipe	20.6	20 (508)	0.040	0.1	426	0.87
Pipe X	15.9	26 (660.4)	0.024	0.15	498	0.81
Pipe Y	19.1	16 (406.4)	0.047	0.15	538	0.91

3.2 Fracture toughness

The fracture toughness values for the pipes were evaluated following the ASTM E1820-22 and CSA CHMC 1-2014 standards [6] and are listed in Table 2. Fracture toughness at 100 bar H_2 was evaluated with a monotonically increasing stress intensity, i.e., K-rate of 0.1 MPa√m/min, except for the γ-Pipe which was tested with an increasing K-rate of 0.3 MPa√m/min both at 100 bar H_2 and 80% N2/20% H_2 gas mixture (100 bar). The tests in air were performed with a K-rate of 3.8 MPa√m/min. The fracture toughness results in Table 2 suggest that all the materials are somewhat susceptible to HE and suffers some mechanical performance degradation in H_2 environment. Nevertheless, the performance of all the materials qualifies the toughness requirements as per the ASME B.31.12 design code [7] , comfortably, for H_2 pipeline usage. The fracture toughness obtained at 20 bar H2 (partial pressure) is twice to that of γ-Pipe sample tested in 100 bar H_2. On the other side, Pipe X performs better than Pipe Y in the same H_2 environment at 100 bar. However, the performance of γ-Pipe and Pipe Y at 100 bar H_2 is similar in terms of both fracture toughness and crack growth resistance (Fig. 2 (a)), even though, they have significantly different YS levels. These behaviours are further investigated in the upcoming sections.

Table 2 - Fracture toughness properties of the pipes

Material	Environment	Fracture toughness, $K_{JQ0.2}$ (MPa√m)	Additional measurements		
			$J_{Q0.2}$ (kJ/m²)	J_{th} (kJ/m²)	K_{Jth} (MPa√m)
Gamma-Pipe (γ-Pipe)	Air	267	315	249	238
	H_2 (100 bar)	82	30	20	67
	80% N_2+20% H_2 (100 bar)	160	113	79	134
Pipe X	Air	--	--	--	--
	H_2 (100 bar)	116	59	48	104
Pipe Y	Air	191	160	29	81
	H_2 (100 bar)	91	36	27	79

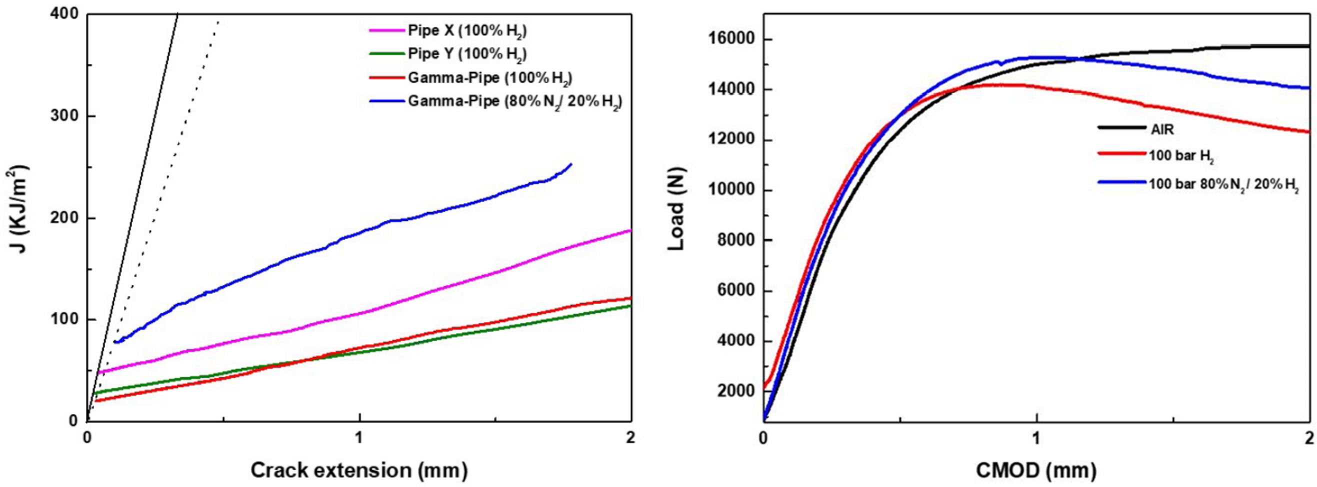

Figure 2 - (a) J-integral vs. crack extension (J-R) curves for all the materials at 100 bar H_2. (b) Load vs crack mouth opening displacement (CMOD) plots in air, 100 bar H_2 and 20 bar H_2 (partial pressure) for γ-Pipe, shown as an example

3.3. Fractography

Fractography was performed on the fracture toughness tested samples for the investigation of the fracture mode in these materials. The stretch zone associated with the crack initiation process and the extension zone associated with the crack propagation were investigated, lying in the crack plane while progressing through the longitudinal cross-section of the sample. Fig. 3 shows stereo and depth field images of the fracture surface for Pipe X, tested in H_2 (100 bar). Fracture surface mapping was performed along the primary crack direction (also rolling direction, RD) while rastering from left to right in the crack plane.

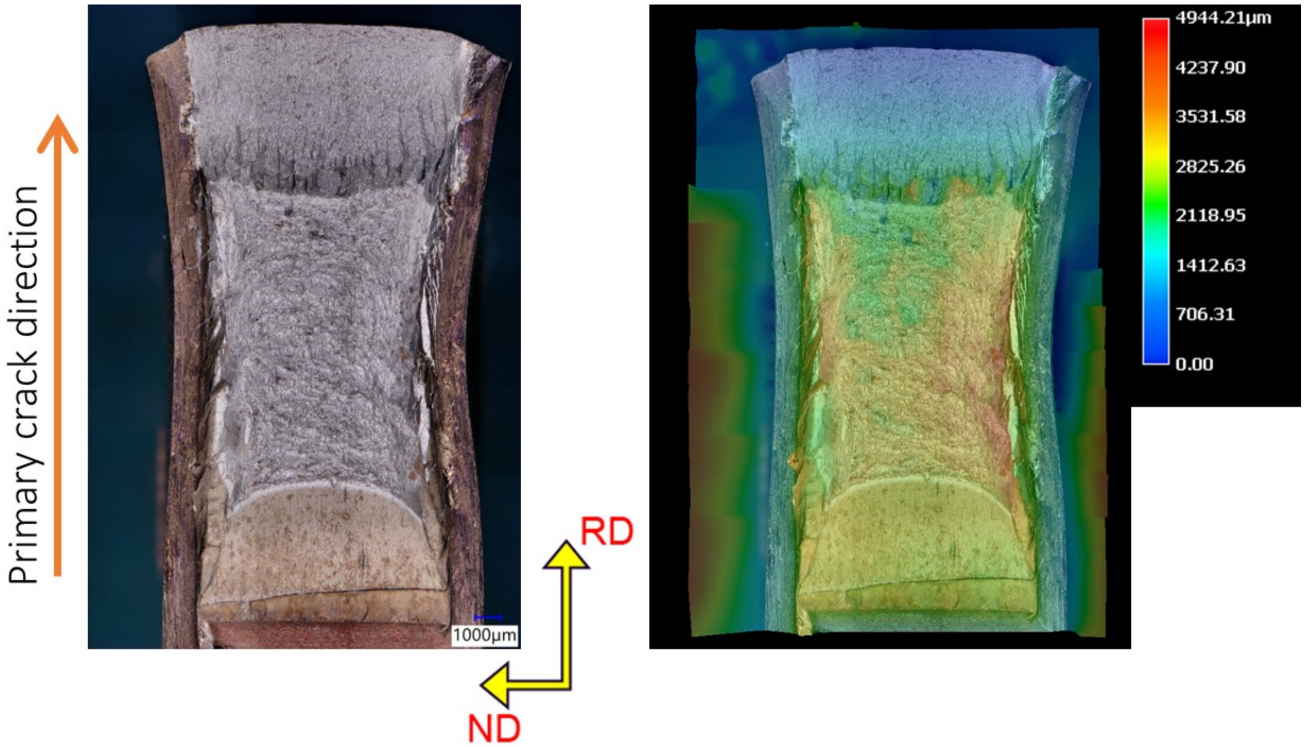

Figure 3 - Stereo and depth field image (top view) of the Pipe X fracture surface

A comparison of the stretch zone at the interface of fatigue pre-crack and crack extension, between γ-Pipe tested in 100 bar and 20 bar H_2 (partial pressure) is shown in Fig. 4. In both of the cases, the presence of stretch zone is diminished into a boundary due to the influence of hydrogen. A planar transition at the intersection of fatigue pre-crack and crack extension occurs in the direction of primary crack propagation as can be seen in case of γ-Pipe at 20 bar H_2 (partial pressure), with some presence of ductile dimple morphologies. Some fine out-of-plane "secondary cracks" perpendicular to the direction of primary crack can also be observed in the stretch zone. On the other hand, the stretch zone (or stretch boundary) in the case of γ-Pipe at 100 bar H_2 is entirely flat with relatively large secondary cracks marked by yellow arrows, showing the severity of failure. This observation directly corresponds to the fracture toughness measurements.

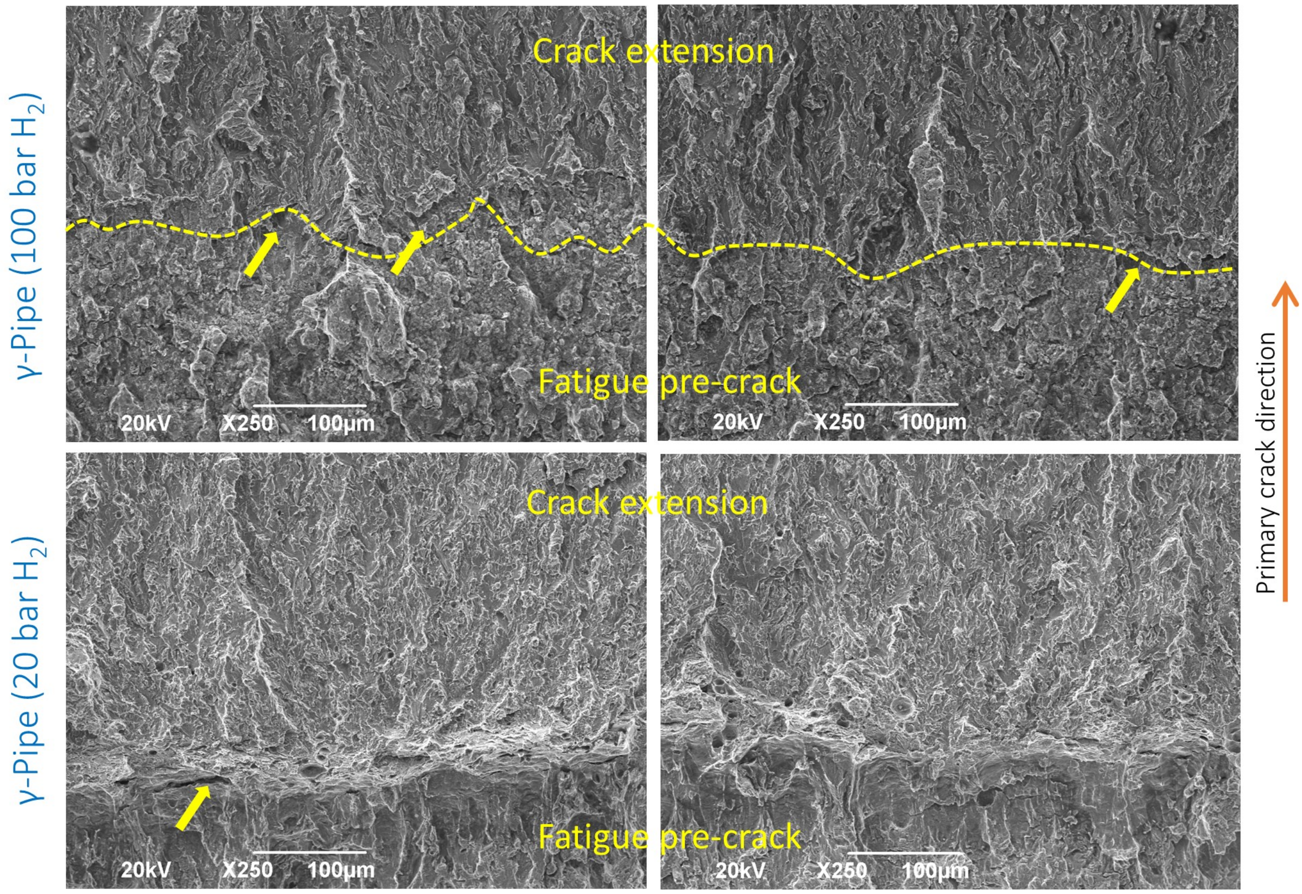

Figure 4 - Fracture surface mapping of fatigue pre-crack and crack extension interface for γ-Pipe

Similar comparisons were made between the pipes, Pipe X and Pipe Y, as shown in Fig. 5. The stretch zone in Pipe X (with higher fracture toughness) shows a clear planar transition between the fatigue pre-crack and crack extension zone with very fine secondary cracks, like γ-Pipe tested in 20 bar H_2 (partial pressure). However, the stretch zone in Pipe Y is vanishingly small showing an entirely flat surface with multiple large secondary cracks. Thus, good agreements were observed between Pipe Y and γ-Pipe tested in 100 bar H_2 both in terms of fracture surface observation and fracture toughness measurements. The origin of secondary crack formation in Pipe Y was further investigated through the characterization of focused ion beam (FIB) lift-out lamellae machined from the fracture surfaces.

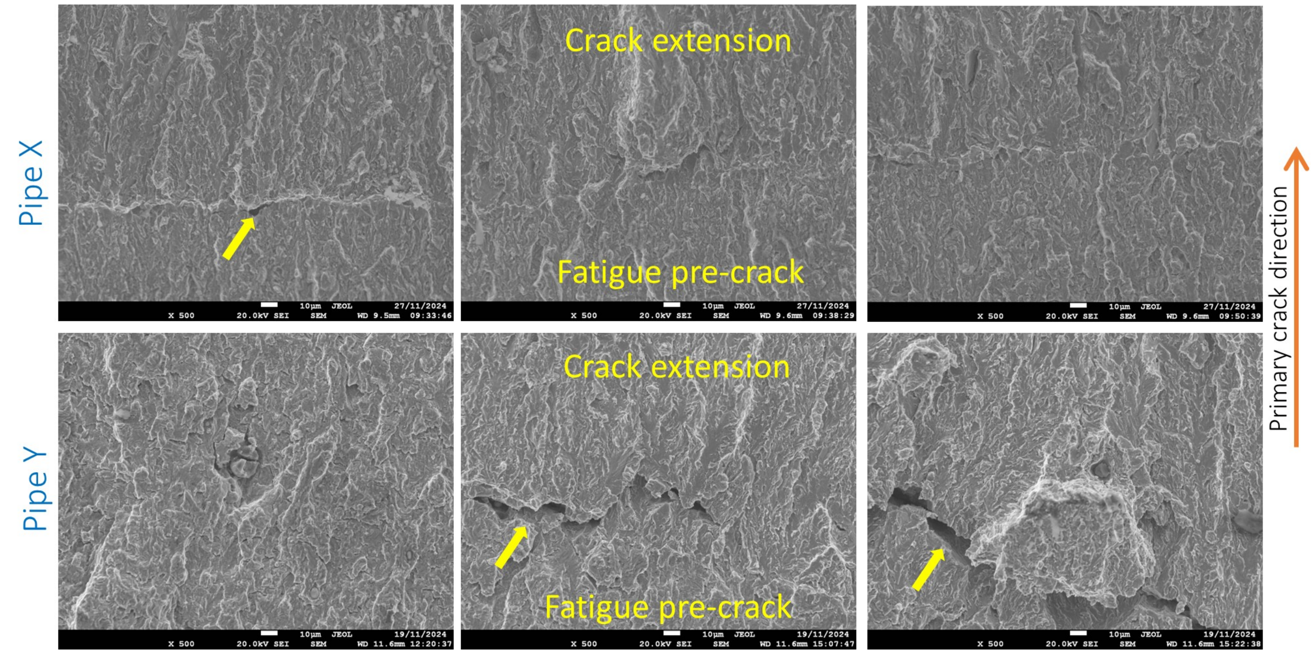

Figure 5 - Fracture surface mapping of fatigue pre-crack and crack extension interface for Pipes: X and Y

4. DISCUSSION

The higher fracture toughness of γ-Pipe tested in 20 bar H_2 (partial pressure) compared to the 100 bar tested sample shows a clear indication on the effect of H_2 partial pressure on fracture toughness, as reported earlier [2][3] . Availability of higher hydrogen concentration at the crack-tip due to higher H_2 pressure leads to increased degree of embrittlement. However, the fracture touhghness differences between Pipe X, Pipe Y and γ-Pipe tested in 100 bar H_2 cannot be directly related to the differences in their YS. For instance, the YS of Pipe Y is signficantly higher than γ-Pipe but their fracture toughness values are similar. Thus, the influence of pipe formation mechanics in terms of "thickness-to-outer diameter" ratio, (t/OD), was investigated. The strain from the pipe forming process (using coils) may potentially increase hydrogen embrittlement (HE) susceptibility through multiple interconnected mechanisms, such as, plastic deformation, residual stresses, and or microstructural changes [8][9] . The "t/OD" ratio could play a role as a design parameter affecting the strain distribution in HFI welded pipes, although further investigation is required to better understand these relationships. Simply speaking, the strain during a pipe forming process scales with t/OD ratio [10][11] . However, research suggests that a threshold effect exists in pipe forming mechanics, with critical transitions occurring around t/OD ratios of 0.025-0.035, where linear behaviour breaks down switching to exponential [11][12][13] . This threshold marks the boundary where geometric nonlinearity begins to control the deformation process rather than material properties alone. Pipe X having a low t/OD ratio of 0.024 shows higher fracture toughness and crack growth resistance in 100 bar H_2 while Pipe Y and γ-Pipe having a t/OD ratio higher than 0.035 shows higher susceptibility, thus overruling the influence of strength on susceptibility. The increased HE susceptibility could be due to an increase in dislocation density from the pipe forming strain which again could serve as reversible traps for hydrogen. This, in turn, might enhance effective hydrogen concentration followed by absorption near the crack tip, potentially facilitating quicker crack initiation and propagation during fracture toughness testing. The stress-state along with hydrogen concentrations at the crack tip were estimated by developing a stress coupled hydrogen diffusion finite element model in ABAQUS. The stress triaxiality and total hydrogen concentration at the crack-tip of the γ-Pipe (20 bar H_2 partial pressure) is shown in Fig. 6 as an example.

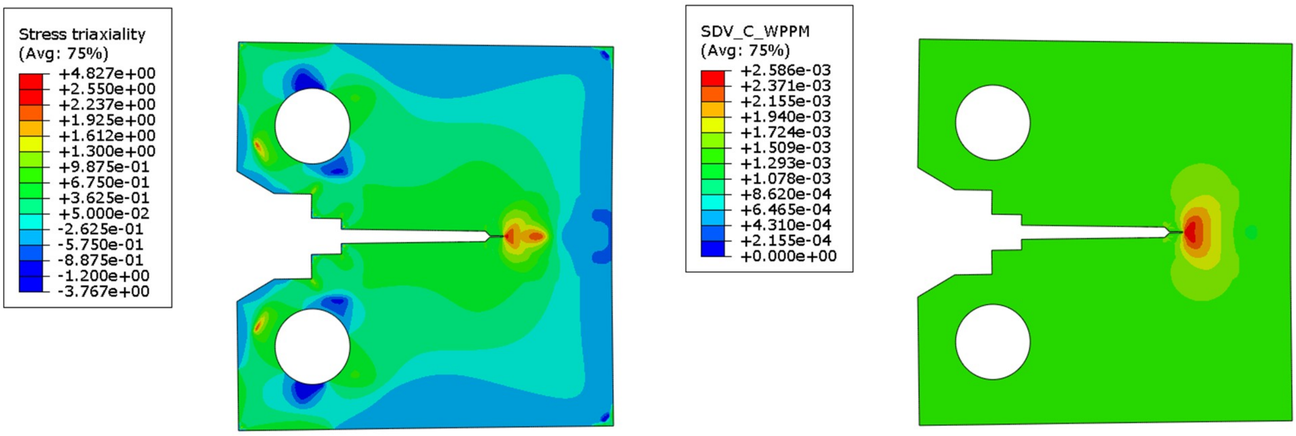

Figure 6 - 2D surface map showing stress triaxiality and total hydrogen concentration at the crack-tip for γ-Pipe (20 bar H_2 partial pressure) during crack initiation using FEA

The fracture toughness behaviour correlates well with the fracture surface mapping, where multiple large out-of-plane “secondary cracks” was observed in the stretch boundary (Pipe Y, in particular), as discussed in the last section. The out-of-plane secondary cracks perpendicular to the primary crack direction (also rolling direction) was observed in the stretch boundary and crack extension zones. However, the origin of these cracks remains unclear. As a result, they were investigated by leveraging advanced characterization techniques considering Pipe Y as an example case. For this purpose, samples (<200 nm thickness) were machined using the focused ion beam (FIB) technique from stretch zone in the fracture surface of Pipe Y, for transmission electron microscopy (TEM) and electron backscattered diffraction (EBSD). Earlier researchers have reported the local microstructural evolution beneath the fracture surface in H_2 following the fatigue testing of a ferritic-pearlitic low carbon steel [14] . Refined microstructural features were observed around the secondary crack area from TEM characterization as shown in Fig. 7. These features could be identified as dislocation cells comprising of dislocations surrounded by low angle dislocation cell boundaries (marked by red arrows in Fig. 7), generated due to excessive accumulation of dislocations. The low angular misorientation (< 2°) of the dislocation cell boundaries was further confirmed from transmission Kikuchi diffraction (TKD) combined with kernel angular misorientation (KAM). Observation of similar dislocation cells underneath the fracture surface was earlier reported from fatigue tests in H_2 and has been related to hydrogen enhanced localized plasticity (HELP) mechanism [14] . The fact that they are related to hydrogen can be asserted from the observation of the dislocation cells in the vicinity of the secondary crack. Hydrogen enhancing dislocation mobility and rapid accumulation resulting in localized plasticity and softening could ultimately lead to the secondary crack formation as per HELP [15] . It is also possible that alongside HELP, multiple mechanisms are at play, such as, adsorption-induced dislocation emission (AIDE) and hydrogen enhanced decohesion (HEDE) [16] . However, their possible role and involvement will be investigated further. The role of hydrogen leading to these secondary cracks are further confirmed from the TEM characterization of another FIB lamella from the fracture surface of an air tested Pipe Y sample. Similar to the H_2 tested case, the FIB machining was performed close to the stretch boundary (from the fracture surface). However, no such dislocation cell formation was observed. The grains appear to be elongated (or stretched) and somewhat deformed in the thickness (or normal) direction. Such morphology underneath the fracture surface could be related to the shearing of the grains during crack initiation and propagation, which are a sign of ductile fracture experienced by the material in air. Thus, the difference in morphology just beneath the fracture surface between the air and environment tested cases further confirms the mechanistic insights on hydrogen mediated secondary crack formation during the environmental test.

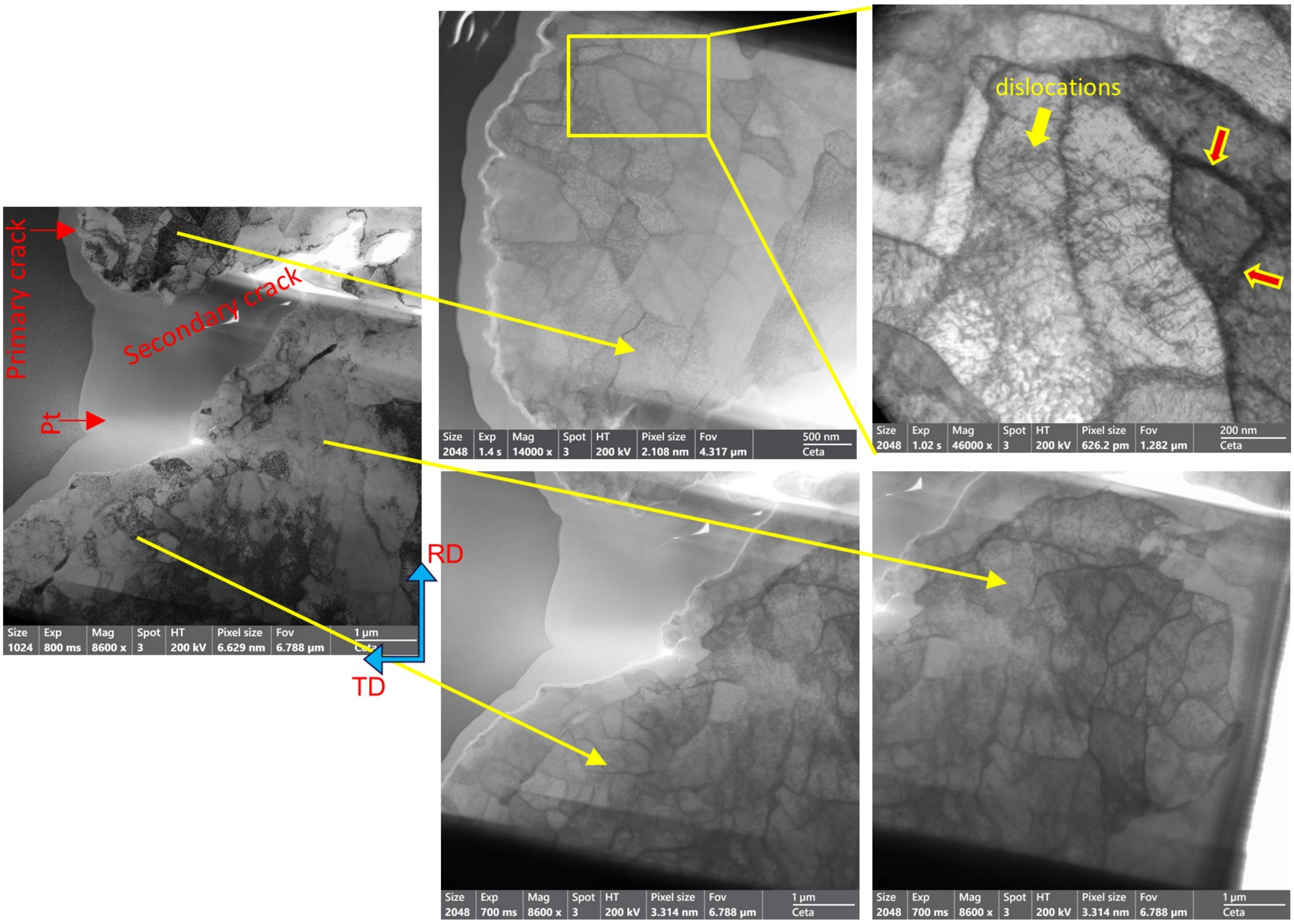

Figure 7 - TEM images of the FIB lamella showing dislocation cells in Pipe Y tested in 100 bar H_2

Additional efforts were made to quantify the secondary cracks observed in the stretch and crack extension zones using a computer vision approach. An algorithm was developed to assess the amount (area fraction) of cracks and their direction from the images. By using Gabor kernels to filter the images, sharp darker areas in the image can be located, as shown as an illustration in Fig. 8. The Gabor filtering also picks up unrelated specks in the image, in addition to cracks. These could add noise to the signal and thus measures were taken to filter-out those noises based on neighbouring pixel contrast. The crack areas usually follow a log-normal distribution, and the specks can be identified as outliers on the lower end of the distribution spectrum to be filtered out using a low-end cut-off filter. The result is denoted as 'filtered' for the corresponding cases (Fig. 9). And from those quantifications, it can be observed that γ-Pipe tested in 100 bar has higher area fraction of secondary cracks compared to 20 bar H_2 (partial pressure). This observation also corresponds to the KJQ0.2 and slope of the J-R curves (Fig. 2). Thus, it can be stated that higher secondary crack formation leads to lower crack initiation and growth resistance in H_2. This technique is a proof of concept and will be refined further to be used for other cases.

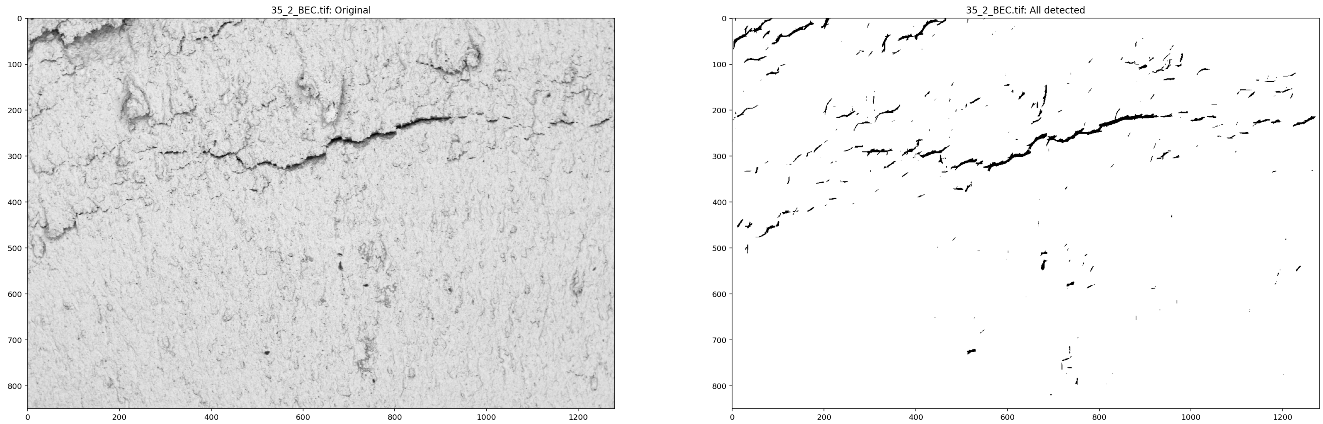

Figure 8 - Binary converted image from BSE fracture surface image using computer vision

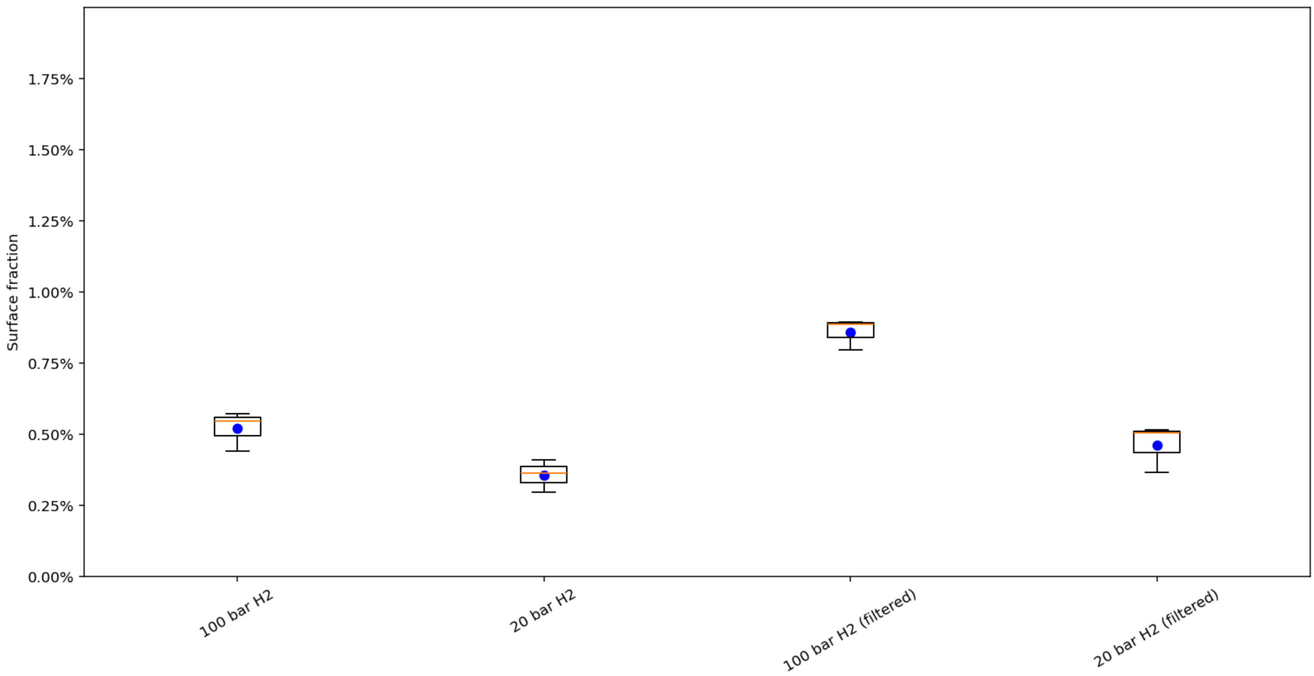

Figure 9 - Area fraction (amount) of secondary cracks at 100x for γ-Pipe tested in 20 & 100 bar H2 using a computer vision approach

5. CONCLUSIONS

Some of the important conclusions from the study are as follows:

1. The significant negative impact of H2 pressure was evident from fracture toughness measurements of γ-Pipe tested at two different pressures.

2. A good correlation was observed between fracture toughness results and fracture modes and morphologies. Pipe Y and γ-Pipe (100 bar H2) with lower fracture toughness exhibit more large-size secondary cracks at the stretch zone (boundary) compared to Pipe X.

3. Higher susceptibility of Pipe Y and γ-Pipe (100 bar H_2) compared to Pipe X could be linked to the differences in their "t/OD" ratios. The higher dislocation density associated with the strain accumulation from pipe forming process could potentially influence hydrogen absorption behaviour and thus HE susceptibility. However, more investigation is necessary for a clear overview on the relationship between pipe geometry, forming-induced microstructural changes and HE.

4. The out-of-plane secondary cracks are a result of hydrogen mediated fracture. High density of dislocation cell formation with localized dislocation accumulation was observed along the secondary crack area in FIB lamella from the fracture surface. This indicates hydrogen enhanced localized plasticity and softening related to HELP mechanism.

5. Computer vision approach indicates lower crack growth resistance in H_2 could be due to more secondary crack formation.

ACKNOWLEDGEMENTS

The authors would like to acknowledge Davit Melkonyan, Vahid Samaee and John Vande Voorde, research engineers at ArcelorMittal Global R & D Gent (OCAS), for their contribution with FIB & TEM characterization and crack area analysis (using computer vision), respectively. The authors would also like to acknowledge Wahib Saikaly, department manager (Metallurgy) at ArcelorMittal Global R & D Gent (OCAS) for his valuable remarks during the manuscript preparation.

REFERENCES

[1] Global Hydrogen Review 2024, International Energy Agency.

[2] Topolski, K., Reznicek, E.P., Erdener, B.C., San Marchi, C.W., Ronevich, J.A., Fring, L., Simmons, K., Fernandez, O.J.G., Hodge, B.M. and Chung, M., 2022. Hydrogen blending into natural gas pipeline infrastructure: Review of the state of technology.

[3] Mechanical Testing Phase 1, H2PIPE JIP - Design and Operation of Hydrogen Pipelines, DNV, 2023.

[4] ASTM E1820-22: Standard Test Method for Measurement of Fracture Toughness, American Society for Testing and Materials, 2022.

[5] ISO 4967, Determination of content of nonmetallic inclusions, International Standardization Organization, 2013.

[6] CSA CHMC 1-2014, Canadian Standards Association, 2014.

[7] ASME B31.12-2019, Hydrogen Piping and Pipelines: ASME Code for Pressure Piping, American Society of Mechanical Engineers, 2019.

[8] Tekkaya, B., Dölz, M. and Münstermann, S., 2024. Multi-scale approach to hydrogen susceptibility based on pipe-forming deformation history. International Journal of Mechanical Sciences, 282, p.109625.

[9] Kraegeloh, J., Bosch, C., Brauer, H. and Kulgemeyer, A., 2011, March. Effect of residual stresses on the HIC resistance of ERW pipes for line pipe applications. In CORROSION 2011 (pp. 1-11). Association for Materials Protection and Performance.

[10] Mjaku, M., Calculation of Stresses and Strain with the Analytical Method of Pipes in High Frequency Longitudinal Welded Pipes: Calculation of Stresses and Strain with the Analytical Method of Pipes in High Frequency Longitudinal Welded Pipes. Technium, 2(6), pp.1-13.

[11] Kim, D.W., Kim, W.K., Bae, J.H., Choi, W.D., Kim, H.S. and Lee, S., 2019. Yield-strength prediction of flattened steel pipes by competing Bauschinger effect and strain hardening during pipe-forming. Scientific Reports, 9(1), p.14002.

[12] Rukavishnikova, V.A. and Tkachenkoa, O.P., 2021. Limit states of a stress-strain pipeline. In CEUR Workshop Proceedings (pp. 54-66).

[13] Li, J., Zhou, C.Y. and Zhu, J.G., 2020. Limit loads for 180 pipe bends under in-plane bending moment considering geometric nonlinearity. International Journal of Pressure Vessels and Piping, 183, p.104100.

[14] Wang, S., Nagao, A., Sofronis, P. and Robertson, I.M., 2018. Hydrogen-modified dislocation structures in a cyclically deformed ferritic-pearlitic low carbon steel. Acta Materialia, 144, pp.164-176.

[15] Robertson, I.M., 1999. The effect of hydrogen on dislocation dynamics. Engineering fracture mechanics, 64(5), pp.649-673.

[16] Lynch, S., 2012. Hydrogen embrittlement phenomena and mechanisms. Corrosion reviews, 30(3-4), pp.105-123.